Available online at www.sciencedirect.com
ScienceDirect
Earth and Planetary Science Letters 259 (2007) 256–265
EPSL
www.elsevier.com/locate/epsl

Imaging ruptured lithosphere beneath the Red Sea and Arabian Peninsula

Samantha E. Hansen [a,b,*], Arthur J. Rodgers [b], Susan Y. Schwartz [a], Abdullah M.S. Al-Amri [c]

[a] Earth and Planetary Sciences Department, University of California, Santa Cruz, 1156 High St., Santa Cruz, CA, 95064, USA
[b] Energy and Environment Directorate, Lawrence Livermore National Laboratory, 7000 East Ave., Livermore, CA, 94551, USA
[c] Geology Department and Seismic Studies Center, King Saud University, P.O. Box 2455, Riyadh, 11451, Saudi Arabia

Received 26 February 2007; received in revised form 23 April 2007; accepted 25 April 2007
Available online 3 May 2007
Editor: R.D. van der Hilst

Abstract

The Red Sea Rift, an archetype of a newly formed ocean basin, is an ideal environment in which to study the controversial processes associated with continental rifting. Different models have been proposed to explain how rifting in the Red Sea evolved; however, accurate constraints on lithospheric structure have not been available to discriminate rifting models. We use the S-wave receiver function technique to produce the first images of the lithosphere–asthenosphere boundary (LAB) structure along the Red Sea and throughout the Arabian Peninsula. Lithospheric thickness varies considerably, with thin lithosphere centered on the rift axis, thickening toward the Arabian interior. Gravity data are well fit by our structural model and indicate that high surface topography along the rift flank is not in isostatic equilibrium, requiring dynamic compensation for its support. While our derived structure is consistent with active rifting processes, previous studies demonstrated that the Red Sea initiated as a passive rift. Therefore, our results suggest a two-stage rifting history, where extension and erosion by flow in the underlying asthenosphere are responsible for variations in LAB depth. LAB topography guides asthenospheric flow beneath western Arabia and the Red Sea, demonstrating the important role lithospheric variations play in the thermal modification of tectonic environments.

Keywords: Arabia; Red Sea; rifting; lithosphere–asthenosphere boundary; S-receiver functions

1. Introduction

Rifting of the Red Sea began about 30 million years ago, separating the western edge of the Arabian Plate from Africa (Camp and Roobol, 1992). Some studies (Wernicke, 1985; Voggenreiter et al., 1988; McGuire and Bohannon, 1989) suggest that the Red Sea developed as a passive rift, where extensional stresses due to far-field body forces are accommodated on low-angle detachment planes extending through the entire lithosphere below the rift (Fig. 1a). This results in passive upwelling of asthenospheric material below the rift and asymmetric thinning, where the thinnest lithosphere is laterally offset from the rift axis. Other studies (McKenzie, 1978;

* Corresponding author. Earth and Planetary Sciences Department, University of California, Santa Cruz, 1156 High St., Santa Cruz, CA, 95064, USA. Tel.: +1 831 459 4426; fax: +1 831 459 3074.
E-mail addresses: shansen@es.ucsc.edu (S.E. Hansen), rodgers7@llnl.gov (A.J. Rodgers), susan@es.ucsc.edu (S.Y. Schwartz), amsamri@ksu.edu.sa (A.M.S. Al-Amri).

0012-821X/$ - see front matter © 2007 Elsevier B.V. All rights reserved.
doi:10.1016/j.epsl.2007.04.035

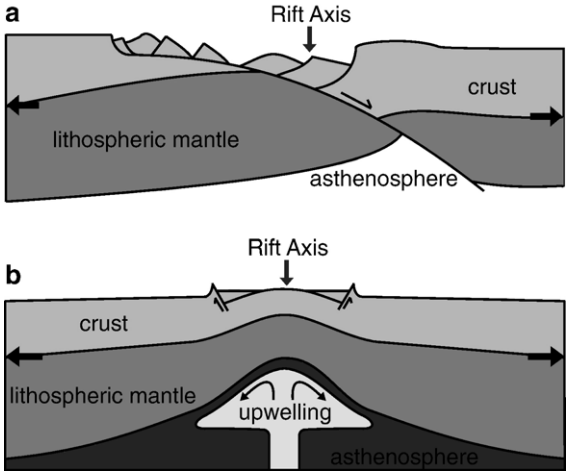

Fig. 1. Schematic end-member rifting models. **a** Passive rifting, where the underlying asthenosphere is passively upwelled and the thinnest lithosphere is offset from the rift axis. **b** Active rifting, where the lithosphere is eroded by asthenospheric flow and the thinnest lithosphere is coincident with the rift axis. The direction of extension is shown by the black, horizontal arrows in both cases.

Bellahsen et al., 2003) argue that the Red Sea is an active rift, where the lithosphere is thermally eroded by flow in the underlying asthenosphere, requiring the presence of hot, ascending material (Fig. 1b). In this case, the rift flanks are thermally uplifted, and the area of greatest lithospheric thinning is coincident with the rift axis. It has also been suggested that these two end-member models are not mutually exclusive; rifting in the Red Sea may have been initiated by passive processes, followed by more recent active processes associated with a mantle upwelling (Camp and Roobol, 1992; Ebinger and Sleep, 1998; Daradich et al., 2003).

The Arabian Peninsula is composed of the western Arabian Shield and the eastern Arabian Platform (Fig. 2). The Shield is composed of Proterozoic island arc terranes that were accreted together 600–900 Ma, and basement rocks in this region have little to no sediment cover. However, the Proterozoic basement rocks in the Platform are covered by up to 10 km of Phanerozoic sediments (Stoeser et al., 1985). Seismic body and surface wave tomography studies (Debayle et al., 2001; Benoit et al., 2003; Julia et al., 2003; Nyblade et al., 2006; Park et al., in press) have shown that the upper mantle beneath the Arabian Shield and the Red Sea is anomalously slow, most likely associated with a shallow lithosphere–asthenosphere boundary (LAB), and that velocities increase towards the continental interior. Additionally, an abrupt change in the lithospheric structure across the Shield–Platform boundary has been inferred (Nyblade et al., 2006; Park

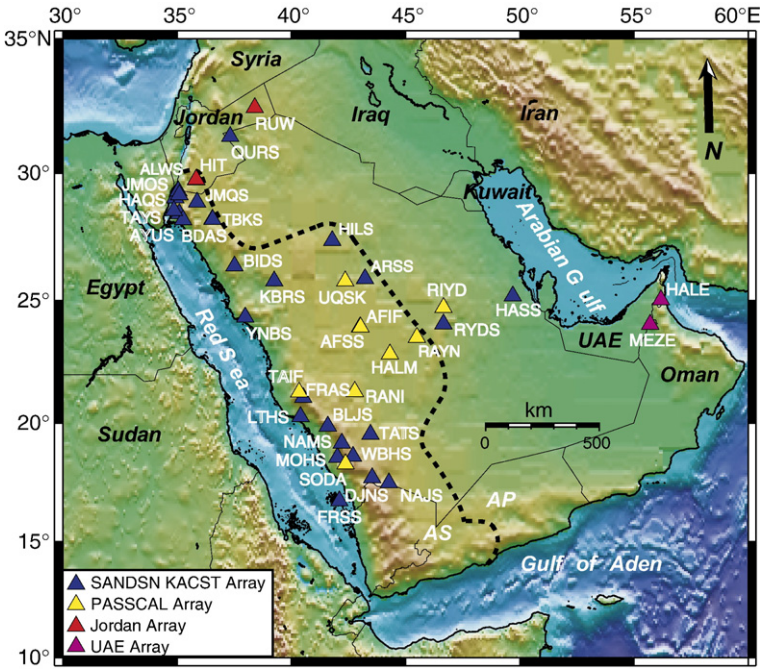

Fig. 2. Station map. The four different colors of triangles indicate the four seismic networks included in this study. SANDSN: blue, IRIS-PASSCAL: yellow, Jordan: red, UAE: pink. The corresponding station names are also listed. The dashed black line shows the boundary between the Arabian Shield (AS) and the Arabian Platform (AP).

et al., in press). Estimates of lithospheric thickness from seismic refraction, P-wave receiver function (PRF), xenolith, and isotope studies vary from about 40 km near the Red Sea coast to about 100 km in the Arabian interior (Mooney et al., 1985; Altherr et al., 1990; Camp and Roobol, 1992; Sandvol et al., 1998). However, these studies do not provide accurate and spatially complete estimates of lithospheric thickness to discriminate the type of rifting occurring in the Red Sea.

In this study, we use the S-wave receiver function (SRF) technique (Farra and Vinnik, 2000; Li et al., 2004; Kumar et al., 2005; Mohsen et al., 2006) to determine the LAB depth by identifying S-to-P (Sp) conversions from discontinuities beneath seismic stations, thereby providing a direct constraint on the lithospheric thickness and new insights into the passive–active rifting debate. Unlike PRFs, where crustal multiples can mask the conversion from the LAB, boundary conversions on SRFs can be more clearly identified because they arrive earlier than the direct S phase while all crustal multiples arrive later. We demonstrate that the lithospheric thickness varies considerably beneath Arabia, with the thinnest lithosphere centered on the Red Sea Rift axis. Our structural model is consistent with gravity data collected by the GRACE satellites (Tapley et al., 2005) and, in conjunction with previous findings, suggests a two-stage rifting history, where extension and erosion by flow in the asthenosphere are responsible for variations in LAB topography.

2. Data and methodology

Teleseismic waveform data recorded by broadband instruments from four different seismic networks were used. The largest array, the Saudi Arabian National Digital Seismic Network (SANDSN), includes 27 broadband stations distributed along the eastern edge of the Red Sea and across the Arabian Peninsula (Al-Amri and Al-Amri, 1999) (Fig. 2, Table 1). SANDSN data from events occurring since 2000 were used for this study. To supplement the SANDSN coverage, we also analyzed data recorded by the eight IRIS-PASSCAL Saudi Arabian Broadband Array stations, which operated from November 1995 to March 1997 (Vernon and Berger, 1998), data from two stations deployed in Jordan, which operated between 1998 and 2001 (Rodgers et al., 2003a), and data recorded by two stations in the UAE from 2003 and 2004 (Rodgers et al., 2003b) (Fig. 2, Table 1).

In general, the receiver function method utilizes coordinate rotation and deconvolution to identify converted phases from seismic discontinuities. To detect Sp conversions, three-component seismic data must be rotated around the incidence angle into the SH–SV–P coordinate system (Li et al., 2004). This rotation is critical because if an incorrect incidence angle is used, noise can be significantly enhanced and major converted phases may become undetectable. In addition, since S-waves have lower frequencies than P-waves, more restrictive event selection and different filtering limits are required for SRF analysis as compared to PRF analysis (Farra and

Table 1
Stacked boundary depths

Station name	Latitude	Longitude	Moho depth (km)	LAB depth (km)
AFIF	23.93	43.04	35	98
AFFS	23.9267	43.0005	33	86
ALWS	29.3103	35.065	29.5	63
ARSS	25.881	43.2365	36	103
AYUS	28.1889	35.2689	24	69
BDAS	28.4317	35.1014	31	62
BIDS	26.867	36.9595	–	–
BLJS	19.8812	41.5992	35	77
DJNS	17.7073	43.5434	45	78
FRAS	21.0622	40.52	–	–
FRSS	16.7392	42.1143	12	62
HALE	25.0911	56.2394	–	–
HALM	22.8454	44.3173	38	118
HAQS	29.0548	34.9297	33	66.5
HASS	25.1899	49.6944	41.5	134
HILS	27.3835	41.7917	39	69
HIT	29.743	35.841	35.5	62.5
JMOS	29.1686	35.1094	29	54
JMQS	28.8861	35.8778	–	–
KBRS	25.7893	39.2623	23	57
LTHS	20.275	40.4107	27	52
MEZE	24.0452	55.8035	44.5	113
MOHS	18.5761	42.019	–	–
NAJS	17.5034	44.2847	–	–
NAMS	19.1714	42.2084	37.5	71
QURS	31.386	37.324	34	61
RANI	21.3116	42.7761	41.5	123
RAYN	23.522	45.5008	35	162
RIYD	24.722	46.6643	47	153
RUW	32.475	38.402	–	–
RYDS	24.19	46.64	–	–
SODA	18.2921	42.3769	38	60
TAIF	21.281	40.349	–	–
TATS	19.5412	43.4775	41.5	82.5
TAYS	28.5511	34.8717	28	61
TBKS	28.2248	36.5485	35	59
UQSK	25.789	42.36	32	106
WBHS	18.6057	42.7144	–	–
YNBS	24.3397	37.9922	28	55

The latitude and longitude of each station is provided, along with the Moho and LAB depths obtained from the stacked SRFs and synthetic fits. A "–" indicates that the depth could not be determined for that particular station either due to either a lack of data or poor signal-to-noise ratios.

Vinnik, 2000; Li et al., 2004; Kumar et al., 2005; Mohsen et al., 2006).

We selected S-waves with high signal-to-noise ratios from earthquakes with magnitudes larger than 5.7 in a distance range of 60° to 85°. Waveforms were first rotated from the N–E–Z to the R–T–Z coordinate system using the event's back-azimuth and were visually inspected to pick the S-wave onset. The three-component records were then cut to focus on the section of the waveform that is 100 s prior to the S arrival and 20 s after. To rotate the data into the SH–SV–P coordinate system, a subroutine was developed, based on the approach of Sodoudi (2005), to determine the correct incidence angle. The cut R–T–Z seismograms are rotated through a series of incidence angles to create a set of quasi-SV and quasi-P data. Each quasi-SV component is then deconvolved from the corresponding quasi-P component using Ligorria and Ammon's iterative time domain method (1999), which creates an SRF. To make the SRFs directly comparable to PRFs, both the time axes and the amplitudes of the SRFs are reversed (Farra and Vinnik, 2000; Li et al., 2004; Kumar et al., 2005; Mohsen et al., 2006). The frequency content of the receiver function is controlled by the Gaussian width factor, a (Ligorria and Ammon, 1999). For PRF analysis, common values of a are about 2.5; however, a smaller a of 1.0 was used for the lower frequency SRF analysis.

To limit our examination to the true P, SV components and their corresponding receiver function, we found the incidence angle that minimizes the direct S-wave energy on the P-component. On the time-reversed receiver functions, the direct S arrival is at 0 s. Therefore, we are only interested in the receiver function whose mean amplitude is closest to zero at zero time. A second algorithm was developed to examine all the generated receiver functions for a given event and determine which record best meets this criterion. The P, SV components and the corresponding receiver function with the appropriate incidence angle are retained, and the remaining records are discarded.

Once receiver functions were generated for all events at an examined station, a move-out correction was applied to the receiver functions to correct for variations in distance between events. Again, to make the SRFs directly comparable to PRFs, we used a reference P-wave slowness of 6.4 s/deg (Farra and Vinnik, 2000; Li et al., 2004; Kumar et al., 2005; Sodoudi, 2005; Mohsen et al., 2006). Each individual receiver function was then visually inspected and compared to previously determined PRFs (Sandvol et al., 1998; Al-Damegh et al., 2005) at the same station to identify the crust–mantle boundary (Moho) conversion. Only SRFs that display a clear Moho conversion at the appropriate time were used for further analysis. These records were then stacked to enhance the LAB conversion (Fig. 3). Stacked SRFs were generated for 29 of the 39 total stations. For the remaining stations, stacks could not be created due to either a lack of data or poor signal-to-noise ratios (Table 1).

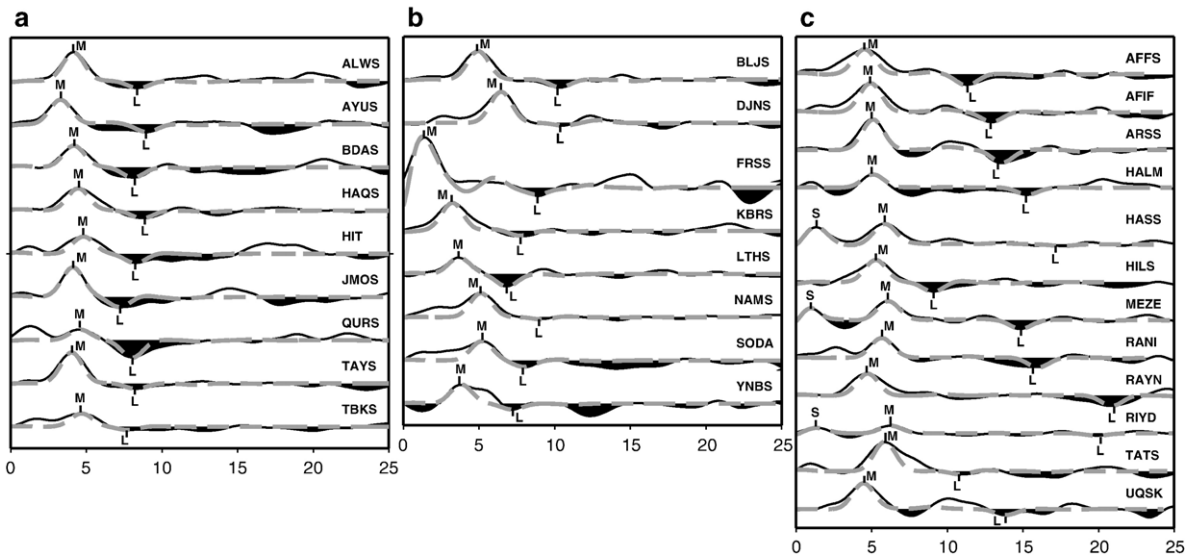

Fig. 3. Example SRFs. The stacked SRFs from individual stations (black) are overlain by their best-fit synthetics (grey dashed lines). Station names are listed on the right. S: sediment-basement boundary, M: Moho, L: LAB. **a** Gulf of Aqaba stations, **b** Red Sea coast stations, **c** Arabian interior stations.

2.1. Synthetic SRFs

The SRF stacks were modeled using synthetic receiver functions generated by the reflectivity method (Randall, 1994). Using published S-wave velocities (V_S) (Sandvol et al., 1998; Rodgers et al., 1999), simple one dimensional models were constructed to match the amplitude and timing of both the Moho and LAB conversions, providing constraints on the velocity contrast and the depths of these boundaries, respectively

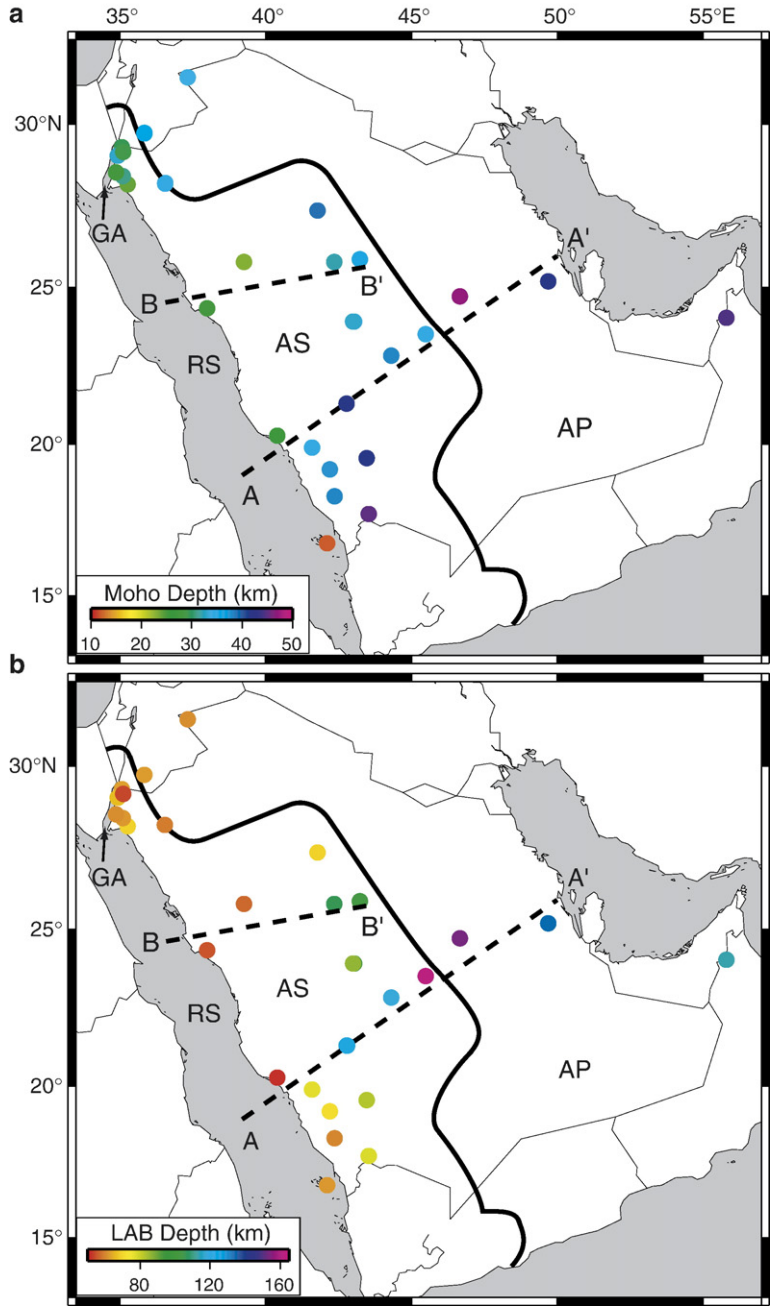

Fig. 4. Maps showing the boundary depths beneath Arabia. The colored circles show the **a** Moho and **b** LAB depths beneath individual stations where warmer colors indicate shallower depths than cooler colors. The solid line marks the boundary between the Arabian Shield (AS) and the Arabian Platform (AP) while the two dashed lines mark the locations of cross-sectional profiles AA′ and BB′ in Figs. 5 and 6. RS: Red Sea, GA: Gulf of Aqaba.

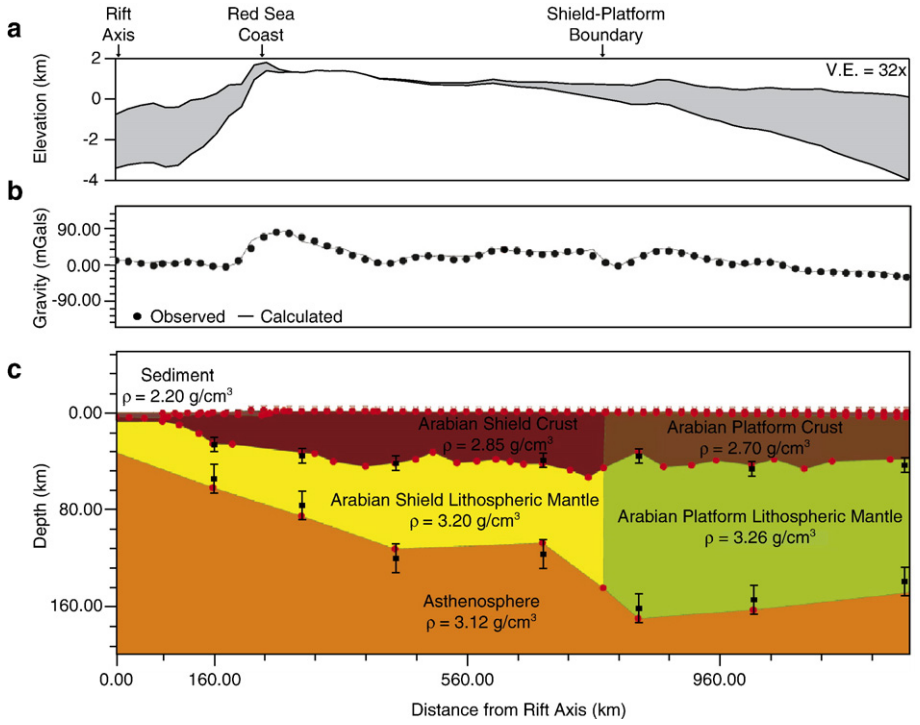

Fig. 5. Topography, gravity signature, and lithospheric structure along cross-sectional profile AA′ from Fig. 4. **a** Topography along the profile plotted with a 32× vertical exaggeration (V.E.). The sediment thickness is shown by the grey shaded areas. **b** Comparison of the observed gravity data from the GRACE satellites (black dots) and the calculated gravity (grey line) resulting from the structural model shown in **c**. Red dots in **c** mark nodes that were used in the gravity modeling to constrain the boundary depths, and the densities (ρ) of each layer are listed. For stations along the profile, the Moho and LAB depths from the SRF analysis are shown by black squares with error bars. The depth errors on the Moho and LAB were 5 and 10 km, respectively, and the boundary depths in the gravity model are well within the error estimates.

(Fig. 3, Table 1). On average, the crustal and upper mantle V_S needed to fit the Moho amplitude were about 3.6 and 4.5 km/s, respectively. These are similar to the V_S used to fit the Moho amplitude on the SANDSN PRFs (Al-Damegh et al., 2005). To fit the LAB amplitude, an average lower mantle V_S of about 4.2 km/s was required. In all cases, a default Poisson's ratio (σ) of 0.25 was used.

It should be noted that the average V_S and default σ used to generate the synthetics differ from those found by waveform modeling. Rodgers et al. (1999) reported average crustal V_S of 3.7 and 3.5 km/s and average upper mantle V_S of 4.3 and 4.55 km/s for the Arabian Shield and Platform, respectively. In addition, the reported σ in the Arabian Shield mantle was 0.29 while in the Platform it was 0.27. Testing revealed that the waveform modeling velocities did not fit the SRF amplitudes as well, but the timing of the phases only changed by a few tenths of a second. Therefore, the difference in V_S only leads to about a 3–5 km difference in depth. However, the timing of the phase conversions is more dependent on σ, where larger values, such as those suggested by the waveform modeling, result in earlier arrivals and shallower discontinuity depths. Based on the amount of variation observed for different values of V_S and σ, the estimated errors for the reported Moho and LAB depths are 5 and 10 km, respectively.

3. Results

Generally, both the Moho and LAB are shallowest near the Red Sea and become deeper towards the Arabian interior (Fig. 4). Given the configuration of stations, the boundary depths along profile AA′ (Fig. 4) are highlighted to examine the structure beneath both the Arabian Shield and Platform. Also, since seafloor spreading is more developed in the southern Red Sea (McClusky et al., 2003), this profile provides a view of the most extensively rifted portion of the lithosphere. However, for comparison, the structure along the more northern profile BB′ (Fig. 4) is also presented.

Near the coast, the Moho depth in southern Arabia increases from about 12 to 35 km, with a few exceptions showing a deeper Moho beneath stations that are

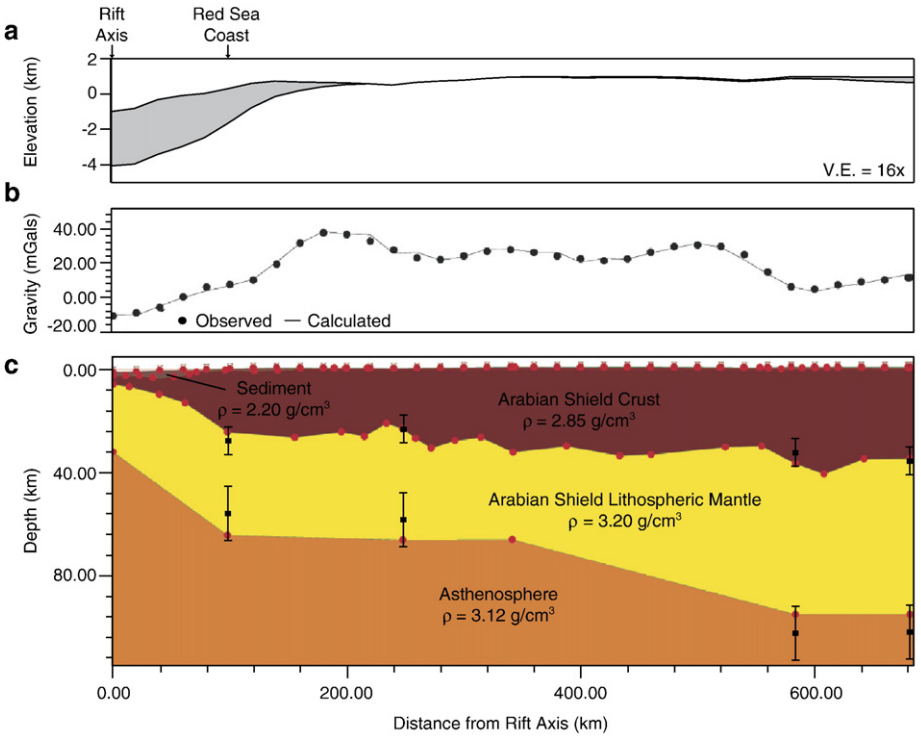

Fig. 6. Topography, gravity signature, and lithospheric structure along cross-sectional profile BB′ from Fig. 4. **a** Topography along the profile plotted with a 16× vertical exaggeration (V.E.). The sediment thickness is shown by the grey shaded areas. **b** Comparison of the observed gravity data from the GRACE satellites (black dots) and the calculated gravity (grey line) resulting from the structural model shown in **c**. Red dots in **c** mark nodes that were used in the gravity modeling to constrain the boundary depths, and the densities (ρ) of each layer are listed. For stations along the profile, the Moho and LAB depths from the SRF analysis are shown by black squares with error bars. The depth errors on the Moho and LAB were 5 and 10 km, respectively, and the boundary depths in the gravity model are well within the error estimates.

situated on higher surface topography along the southern Red Sea coast in the Asir province (ex. stations NAMS, SODA, and DJNS, Fig. 1). The crustal thickening along profile AA′ continues until an average Moho depth of about 40–45 km is reached beneath both the central Arabian Shield and Platform (Fig. 4a). The LAB near the coast is at a depth of about 50 km; however, it rapidly deepens to attain a maximum depth of about 120 km beneath the Arabian Shield within 300 km of the Red Sea. At the Shield–Platform boundary, a step is observed in the lithospheric thickness where the LAB depth increases to about 160 km (Fig. 4b).

Boundary depths along profile BB′ are comparable to those at similar distances along profile AA′. The Moho depth near the coast is about 22–25 km, and crustal thickening continues until an average Moho depth of about 35–40 km is reached beneath the interior Arabian Shield (Fig. 4a). The LAB near the coast is at a depth of about 55 km; however it also deepens beneath the Shield to attain a maximum depth of 100–110 km (Fig. 4b). The broad spatial coverage of these estimates provides the first images of ruptured continental lithosphere on a scale applicable to geodynamical modeling.

3.1. Gravity comparison

The inferred lithospheric structure along both profiles is tested by comparing its predicted gravity signature to data collected by the GRACE satellites (Tapley et al., 2005). Average seismic velocities from both the current and previous studies (Sandvol et al., 1998; Rodgers et al., 1999) were converted to density estimates using the Nafe–Drake relationship (Ludwig et al., 1970) and sediment thickness was extracted from a global sediment model (Laske and Masters, 1997). Along profile AA′, the small-scale (50–200 km) recorded gravity signature can be matched very well by making minor adjustments to the Moho and LAB boundaries (well within the estimated error). Broad-scale gravity observations require a shallow asthenosphere beneath the Red Sea, with the thinnest lithosphere centered on the rift axis (Fig. 5).

Profile BB′ is shorter, has fewer stations and therefore fewer constraints, so we set the lithospheric thickness beneath the rift axis to be similar to that on profile AA′. We then examined if the calculated gravity signature is consistent with the recorded data. Small-scale recorded gravity observations can again be matched very well by slightly adjusting the Moho and LAB boundaries. Broad-scale gravity observations are also well fit by a shallow asthenosphere beneath the Red Sea (Fig. 6). These findings demonstrate that the Moho and LAB SRF results are consistent with gravity measurements across Arabia and support current active rifting processes (Fig. 1b).

4. Discussion and conclusions

The average elevation across Arabia is about 1 km; however, near the Red Sea, the elevation is significantly higher, up to 3 km (Daradich et al., 2003). This high topography is not in isostatic equilibrium with our lithospheric model resulting from the SRF analysis, requiring another compensation mechanism. Potential mechanisms include flexural and dynamic compensation, where the topography is supported by lithospheric rigidity or asthenospheric flow, respectively. Using relationships that described the amplitude of deflection and degree of compensation for a topographic load (Turcotte and Schubert, 2002), we estimate that an elastic thickness of about 20 km is necessary to support the rift flank. Analysis of the East African Rift indicates an elastic thickness less than 10 km (Ebinger and Hayward, 1996). If the elastic thickness of the Red Sea margin is comparable, flexure alone will not support its topography and dynamic compensation must contribute to rift flank support. Daradich et al. (2003) computed mantle flow from seismic tomography and demonstrated that both the rift flank topography and overall tilt of Arabia are dynamically supported.

Both the observed lithospheric thinning and the necessity for dynamic compensation support active rifting processes. In the active rifting model (Fig. 1b), the rift event is preceded by a period of uplift; however, in the passive rifting model (Fig. 1a), associated uplift postdates the rifting event (McGuire and Bohannon, 1989). Geologic and fission track data show that western Arabia was at or below sea level prior to 30 Ma and that the uplift of the Red Sea margin postdates the initiation of rifting by about 5–10 million years (McGuire and Bohannon, 1989). These results demonstrate that the Red Sea began as a passive rift (Wernicke, 1985; Voggenreiter et al., 1988; McGuire and Bohannon, 1989). The mantle temperature beneath the Arabian Shield, determined from xenoliths, is abnormally high, but the surface heat flow is lower than global averages (McGuire and Bohannon, 1989). This suggests that mantle temperatures have not had time to equilibrate at the surface. The thermal disequilibrium, in conjunction with our SRF and gravity results, demonstrate that while active rifting processes are currently affecting the Red Sea, these processes only developed within the last 15–20 million years and therefore reflect a second stage of rifting. This may also explain why the LAB in this region is such a sharp discontinuity. The presence of hot material beneath Arabia associated with active upwelling could lead to some degree of partial melt, which would significantly lower the asthenospheric shear velocity and result in a high velocity contrast across the LAB. It has been suggested that the degree of partial melt beneath Arabia ranges between 4 and 10% (Camp et al., 1991; Camp and Roobol, 1992).

Yuen and Fleitout (1985) illustrated that the convection and heat associated with mantle upwellings, in conjunction with extensional forces, can thin a 100-km-thick lithosphere at an average rate of 7.5 km Myr^{-1}. Using this rate and approximating the starting lithospheric thickness to be about 160 km (the thickness of the lithosphere at the Shield–Platform step), the resulting, thinned lithosphere would have a thickness of about 50 km. This estimate agrees well with our observed lithospheric thickness along the Red Sea coast and demonstrates that active rifting forces could have generated the observed LAB topography over the last 15–20 Myr.

Therefore, our observations of lithospheric structure support a two-stage rifting history along the Red Sea and suggest that the LAB topography is the result of extension and erosion caused by asthenospheric flow. Previous studies (Ebinger and Sleep, 1998; Daradich et al., 2003) speculated at the existence of such topography and suggested that it may direct asthenospheric flow beneath the Arabian Shield and the Red Sea Rift. Inferred flow direction from shear-wave splitting results is also consistent with this conclusion (Hansen et al., 2006). In addition, body and surface wave tomography (Nyblade et al., 2006; Park et al., in press) suggest that the mantle lithosphere beneath the Arabian Shield has been thermally modified and that there is an abrupt change in lithospheric structure across the Shield–Platform boundary. This structural change is also observed in the gravity data (Fig. 5b), where the transition from the Shield to the Platform is marked by a small-scale gravity anomaly. The LAB step imaged in this study may reflect the pre-existing lithospheric thickness prior to the accretion of island arc terranes

composing the Arabian Shield. This step and the rapid lithospheric thinning near the rift likely channelize hot asthenospheric flow as predicted (Ebinger and Sleep, 1998; Daradich et al., 2003; Hansen et al., 2006) and illustrate the important role lithospheric variations play in the thermal modification of tectonic environments.

Acknowledgements

We thank Chuck Ammon for providing the deconvolution and reflectivity programs and Christel Tiberi for her thorough critique of this manuscript. Partial support for this study was provided by CSIDE-IGPP at the University of California, Santa Cruz. This work was performed under the auspices of the U.S. Department of Energy by University of California, Lawrence Livermore National Laboratory under contract W-7405-Eng-48. This is LLNL contribution UCRL-JRNL-226434.

References

Al-Amri, M., Al-Amri, A., 1999. Configuration of the seismographic networks in Saudi Arabia. Seismol. Res. Lett. 70, 322–331.

Al-Damegh, K., Sandvol, E., Barazangi, M., 2005. Crustal structure of the Arabian Plate: new constraints from the analysis of teleseismic receiver functions. Earth Planet. Sci. Lett. 231, 177–196.

Altherr, R., Henjes-Kunst, F., Puchelt, H., Baumann, A., 1990. Volcanic activity in the Red Sea axial trough — evidence for a large mantle diapir. Tectonophysics 150, 121–133.

Bellahsen, N., Faccenna, C., Funiciello, F., Daniel, J.M., Jolivet, L., 2003. Why did Arabia separate from Africa? Insights from 3-D laboratory experiments. Earth Planet. Sci. Lett. 216, 365–381.

Benoit, M., Nyblade, A., VanDecar, J., Gurrola, H., 2003. Upper mantle P wave velocity structure and transition zone thickness beneath the Arabian Shield. Geophys. Res. Lett. 30, 1–4.

Camp, V., Roobol, M., 1992. Upwelling asthenosphere beneath western Arabia and its regional implications. J. Geophys. Res. 97, 15255–15271.

Camp, V., Roobol, M., Hooper, P., 1991. The Arabian continental alkali basalt province, part II, Evolution of Harrats Khaybar, Ithnayn, and Kura, Kingdom of Saudi Arabia. Geol. Soc. Amer. Bull. 103, 363–391.

Daradich, A., Mitrovica, J., Pysklywec, R., Willett, S., Forte, A., 2003. Mantle flow, dynamic topography, and rift-flank uplift of Arabia. Geology 31, 901–904.

Debayle, E., Leveque, J., Cara, M., 2001. Seismic evidence for a deeply rooted low-velocity anomaly in the upper mantle beneath the northeastern Afro/Arabian continent. Earth Planet. Sci. Lett. 193, 423–436.

Ebinger, C., Hayward, N., 1996. Soft plates and hot spots: views from afar. J. Geophys. Res. 101, 21859–21876.

Ebinger, C., Sleep, N., 1998. Cenozoic magmatism throughout east Africa resulting from impact of a single plume. Nature 395, 788–791.

Farra, V., Vinnik, L., 2000. Upper mantle stratification by P and S receiver functions. Geophys. J. Int. 141, 699–712.

Hansen, S., Schwartz, S., Al-Amri, A., Rodgers, A., 2006. Combined plate motion and density driven flow in the asthenosphere beneath Saudi Arabia: evidence from shear-wave splitting and seismic anisotropy. Geology 34, 869–872.

Julia, J., Ammon, C., Herrmann, R., 2003. Lithospheric structure of the Arabian Shield from the joint inversion of receiver functions and surface-wave group velocities. Tectonophysics 371, 1–21.

Kumar, P., Kind, R., Hanka, W., Wylegalla, K., Reigber, C., Yuan, X., Woelbern, I., Schwintzer, P., Fleming, K., Dahl-Jensen, T., Larsen, T., Schweitzer, J., Priestley, K., Gudmundsson, O., Wolf, D., 2005. The lithosphere–asthenosphere boundary in the North-West Atlantic region. Earth Planet. Sci. Lett. 236, 249–257.

Laske, G., Masters, G., 1997. A global digital map of sediment thickness. EOS Trans. AGU 78, F483.

Li, X., Kind, R., Yuan, X., Wolbern, I., Hanka, W., 2004. Rejuvenation of the lithosphere by the Hawaiian plume. Nature 427, 827–829.

Ligorria, J., Ammon, C., 1999. Poisson's ratio variations of the crust beneath North America. Seismol. Res. Lett. 70, 274.

Ludwig, W., Nafe, J., Drake, C., 1970. Seismic refraction. In: Maxwell, A.E. (Ed.), The Sea. Wiley-Interscience, New York.

McClusky, S., Reilinger, R., Mahmoud, S., Ben Sari, D., Tealeb, A., 2003. GPS constraints on Africa (Nubia) and Arabia plate motions. Geophys. J. Int. 155, 126–138.

McGuire, A., Bohannon, R., 1989. Timing of mantle upwelling: evidence for a passive origin for the Red Sea Rift. J. Geophys. Res. 94, 1677–1682.

McKenzie, D., 1978. Some remarks on the development of sedimentary basins. Earth Planet. Sci. Lett. 40, 25–32.

Mohsen, A., Kind, R., Sobolev, S., Weber, M., 2006. DESERT Group, thickness of the lithosphere east of the Dead Sea Transform. Geophys. J. Int. 167, 845–852.

Mooney, W., Gettings, M., Blank, H., Healy, J., 1985. Saudi Arabian seismic refraction profile: a traveltime interpretation of crustal and upper mantle structure. Tectonophysics 111, 173–246.

Nyblade, A., Park, Y., Rodgers, A., Al-Amri, A., 2006. Seismic structure of the Arabian Shield Lithosphere and Red Sea Margin. Margins Newsl. 17, 13–15.

Park, Y., Nyblade, A., Rodgers, A., Al-Amri, A., in press. Upper mantle structure beneath the Arabian Peninsula from regional body wave tomography: implications for the origin of Cenozoic uplift and volcanism in the Arabian Shield, Geochem. Geophy. Geosyst.

Randall, G., 1994. Efficient calculation of complete differential seismograms for laterally homogeneous earth models. Geophys. J. Int. 118, 245–254.

Rodgers, A., Walter, W., Mellors, R., Al-Amri, A., Zhang, Y., 1999. Lithospheric structure of the Arabian Shield and Platform from complete regional waveform modeling and surface wave group velocities. Geophys. J. Int. 138, 871–878.

Rodgers, A., Harris, D., Ruppert, S., Pasyanos, M., Abdallah, A., Al-Yazjeen, T., Al-Gazo, A., 2003a. A broadband seismic deployment in Jordan. Seismol. Res. Lett. 74, 374–381.

Rodgers, A., Lewis, P., Fowler, A., 2003b. A broadband seismic deployment in the United Arab Emirates. Lawrence Livermore National Laboratory Informal Document, vol. UCRL-ID-153713.

Sandvol, E., Seber, D., Barazangi, M., Vernon, F., Mellors, R., Al-Amri, A., 1998. Lithospheric seismic velocity discontinuities beneath the Arabian Shield. Geophys. Res. Lett. 25, 2873–2876.

Sodoudi, F., 2005. Lithospheric structure of the Aegean obtained from P and S receiver functions, PhD Thesis, Freie Universitat Berlin.

Stoeser, D., Camp, V., 1985. Pan-African microplate accretion of the Arabian Shield. GSA Bull. 96, 817–826.

Tapley, B., Ries, J., Bettadpur, S., Chambers, D., Cheng, M., Condi, F., Gunter, B., Kang, Z., Nagel, P., Pastor, R., Pekker, T., Poole, S.,

Wang, F., 2005. GGM02 — an improved earth gravity field model from GRACE. J. Geod. 79, 467–478.
Turcotte, D., Schubert, G., 2002. Geodynamics. Cambridge University Press.
Vernon, F., Berger, J., 1998. Broadband seismic characterization of the Arabian Shield: final scientific technical report. Department of Energy Contract No. F 19628-95-K-0015, vol. 36.
Voggenreiter, W., Hötzl, H., Jado, A., 1988. Red Sea related history of extension and magmatism in the Jizan area (southwest Saudi Arabia): indication for simple-shear during Red Sea rifting. Geol. Rundsch. 77, 257–274.
Wernicke, B., 1985. Uniform-sense normal simple-shear of the continental lithosphere. Can. J. Earth Sci. 22, 108–125.
Yuen, D., Fleitout, L., 1985. Thinning of the lithosphere by small-scale convective destabilization. Nature 313, 125–128.